Theoretical study of the cyclization of α-iminothioaldehydes into dihydrothiazoles

Roger Arnaud,*[a] Nadia Pelloux-Léon,[a] Jean-Louis Ripoll[b] and Yannick Vallée*[a]
[a] *LEDSS, laboratoire associé au CNRS, Université Joseph Fourier, BP 53X, 38041 Grenoble, France*
[b] *Laboratoire de Chimie Moléculaire et Thioorganique, associé au CNRS, ISMRA, 14050 Caen, France*

When synthesized by retro-Diels–Alder reaction under flash vacuum thermolysis conditions, α-iminothioaldehydes undergo a rearrangement to 2,3-dihydro-1,3-thiazoles. These secondary enamines in turn are transformed into the more stable 2,5-dihydro-1,3-thiazoles upon standing in $CDCl_3$ solution. The route from α-iminothioaldehydes to dihydro-1,3-thiazoles has been studied by *ab initio* molecular orbital theory. Geometries of stationary points on the $[C_3H_5NS]$ potential energy surface were optimized using HF/6-31G(d,p) and MP2/6-31(d,p) calculations. Relative energies were estimated using MP4STDQ [and in some cases QCISD(T)] calculations and the 6-31 + G(d,p) basis set and corrected for zero-point vibrational energies. Intrinsic reaction coordinate calculations at HF/6-31G(d,p) level were performed in order to check the profile of the proposed rearrangement. These calculations support the experimental findings. The most energy requiring step was found to be *trans*→*cis* isomerization of the methylimino group [27.8 kcal mol^{-1} at the QCISD(T)/6-31 + G(d,p) level].†

1,3-Thiazoles are the most widely studied S,N-heterocycles.[1] Among their dihydro derivatives, the more easily available are those of the 4,5-dihydro series.[2] The other series, 2,3- and 2,5-dihydro, are little known.[3] In particular, 2,3-dihydro-1,3-thiazoles, without a substituent on the nitrogen atom, were unknown before this work.[4] They are examples of secondary enamines and, as such, can be expected to be readily transformed into their more stable imino tautomers, 2,5-dihydro-1,3-thiazoles. Such isomerization is well documented for simple primary and secondary vinyl amines.[5]

A simple retro-synthetic analysis of 2,3-dihydro-1,3-thiazole (**1a**) (Scheme 1) shows that it could be obtained by a C(2)–S

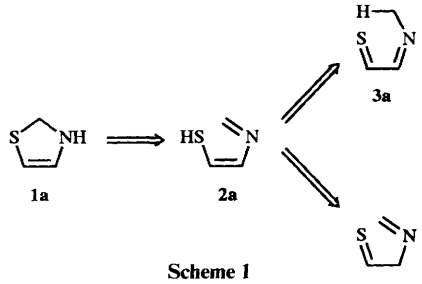

Scheme 1

connection from the enethiol **2a**. This enethiol can be regarded either as the tautomer of *N*-(2-thioxoethyl)methanimine or as the product resulting from a [1,5]-sigmatropic rearrangement of the α-iminothioaldehyde **3a**. Indeed, when in the course of our work on thioaldehydes' reactivity,[6] we tried to synthesize compound **3a**, we observed its cyclization into **1a**.[4] The aim of this paper is to discuss in detail the mechanism leading from α-iminothioaldehydes to dihydrothiazoles.

Synthesis and thermolysis of imines 4a, b

Flash vacuum thermolysis (FVT) has proved to be an efficient technique for the generation and the spectroscopic observation of transient species.[7] Among the reactions that can be used to synthesize reactive thiocarbonyl compounds under FVT conditions, the retro-Diels–Alder reaction[8] is one of the most powerful.[6]

The precursors **4a, b** (Scheme 2) were prepared in two steps

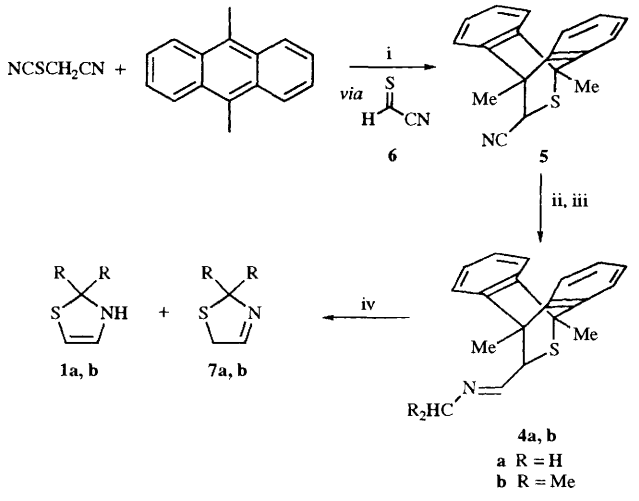

Scheme 2 *Reagents and conditions:* i, Et_3N, $CHCl_3$; ii, DIBAL-H, PhMe; iii, R_2CHNH_2, CH_2Cl_2; iv, FVT, 500 °C, −DMA

from nitrile **5**. This nitrile was obtained by trapping thioformyl cyanide **6**, generated *in situ* by the base induced elimination of HCN from cyanomethylthiocyanate, with 9,10-dimethylanthracene (DMA).[9] Compound **5** was then reduced by DIBAL-H (diisobutylaluminium hydride) to give the corresponding aldehyde, which upon treatment with methyl- or isopropyl-amine gave the two imines **4a, b**.

The thermolysis of these imines was effected at 500 °C. 9,10-Dimethylanthracene condensed immediately at the oven exit, while the obtained volatile products were trapped on a cold finger (liquid N_2) coated with a $CDCl_3$–$CFCl_3$ mixture for NMR analysis. The NMR spectra were recorded at −60 °C. The obtained data, summarized in Scheme 3, clearly demonstrated the formation of the 2,3-dihydro-1,3-thiazoles **1a, b**. The corresponding 2,5-dihydro-1,3-thiazoles **7a, b**[10] were

† 1 kcal mol^{-1} = 4.184 kJ mol^{-1}.

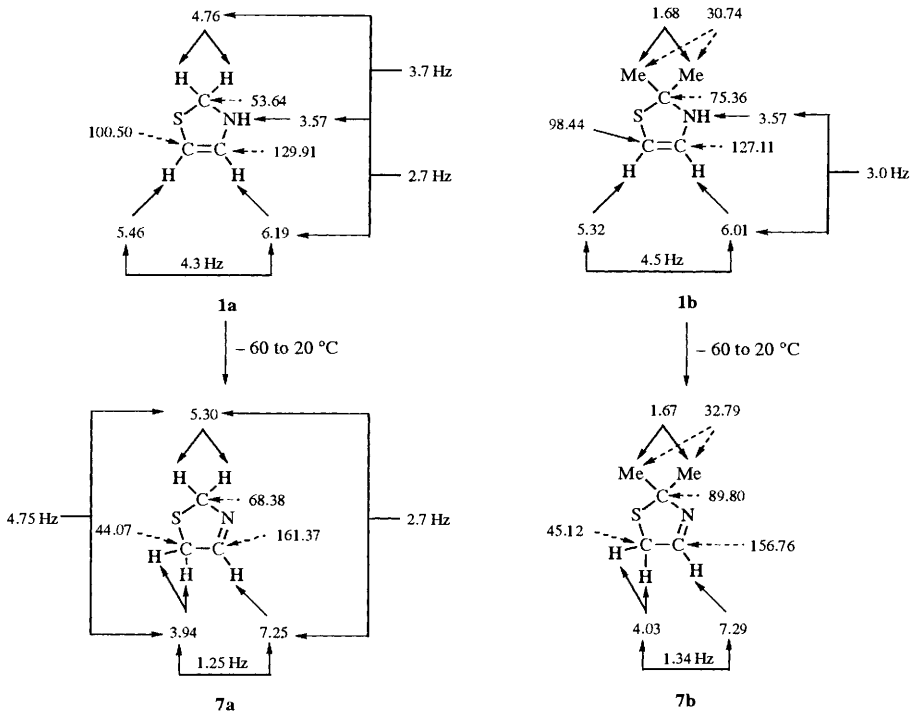

Scheme 3 ^{1}H and ^{13}C NMR chemical shifts δ and coupling constants J_{H-H} of compounds **1a**, **b** and **7a**, **b**

also detected in the spectra (at −60 °C: **1a**:**7a** = 8:1; **1b**:**7b** = 4:1). Upon warming the NMR solution, the secondary enamines **1a**, **b** disappeared and at room temperature the imines **7a**, **b** were observed alone.

Calculations

The calculations were carried out on an IBM RS6000/340 workstation with the GAUSSIAN92 quantum chemical program.[11] Geometries of the stationary points were fully optimized without symmetry constraints at the single determinantal Hartree-Fock (HF) level of theory using the 6-31G(d,p) basis set.[12] Harmonic vibrational frequencies were computed in order to characterize stationary points (minima and first-order saddle points, the latter having exactly one imaginary frequency) and to estimate the zero-point vibrational energy (ZPVE, scaling factor of 0.89) contributions to the relative energies between stationary points.

After transition states were obtained, intrinsic reaction coordinate (IRC)[13] calculations were carried out to follow the reaction path in both directions, leading back to the reactant as to the product. In these calculations, the geometry is optimized at each point along the reaction path as the system decreases in energy to verify that the saddle points obtained were associated with the reaction path originally assumed.

All structures were further optimized at the second order Moller–Plesset perturbation theory [MP2(fc)/6-31G(d,p)] level. Relative energies between stationary points were estimated using total energies computed at the fourth order perturbation theory (MP4SDTQ) and, in some cases, quadratic configuration interaction [QCISD(T)] levels with the 6-31 + G(d,p) basis set[12] using MP2 optimized geometries. The total energies in Hartree of the reference compound **3a** (*trans*,s-*trans*) at the various levels of calculation are as follows: −568.438 20 [HF/6-31G(d,p)], −569.133 20 [MP2/6-31G(d,p)], −569.145 51 [MP2/6-31G(d,p)], −569.221 36 [MP4SDTQ/6 31 + G(d,p)] and −569.223 12 [QCISD(T)/6-31 + G(d,p)].

NBO analyses were performed with the program NBO version 3.1 which was built into link 607 of the GAUSSIAN92 program.[14] Quantitative analysis of the hyperconjugation interactions between various NBOs was obtained using the NBO Fock matrix deletion procedure.[15a] The deletion procedure is not self-consistent, but as long as the particular interactions in the Fock matrix that have been set to zero are not strongly coupled with other interactions, the error in the energy is not significant.[15a] Also, the energies of individual orbital interactions are not strictly additive.[15b]

Results and discussion

Conformers of the α-iminothioaldehyde 3a and their interconversions

Fig. 1 lists selected HF and MP2 parameters of local minima and transition structures involved in this process. The corresponding zero-point vibrational and relative energies are summarized in Table 1. Equilibrium geometries of the s-*trans* isomers are reached for C_s symmetry, while a non-planar structure is obtained for the s-*cis* rotamers. A ∠SCCN dihedral angle of 18.3° (HF) and 14.2° (MP2) is calculated for the *trans*,s-*cis* isomer and of 44° (HF) and 29.4° (MP2) for the *cis*,s-*cis* isomer. The HF and MP2 optimized geometries reported in Fig. 1 show that the absolute values of bond lengths depend on the level of calculation. As it can be seen, inclusion of electron correlation causes a general lengthening of the bond distances, with the exception of the C–C bond which is shortened at the MP2/6-31G(d,p) level by *ca.* 0.01 Å.

Another structural feature of the stable isomers of **3a** is the conformational preference of the methyl group. HF/6-31G(d,p) calculations indicate that the lowest energy conformation has a C–H bond lying in the plane of the C–N–C(H_3) group and eclipsing the C=N bond, while the staggered conformation was characterized as the transition state between two equivalent eclipsed rotamers. The rotational barrier is rather large (2.1 kcal mol^{-1}) in the case of the two s-*trans* isomers. This tendency of the methyl group to eclipse the C=N bond would be attributed to the nitrogen lone pair $n_N \rightarrow$antibond σ^*_{CH} orbital interaction which would be maximized for the eclipsed structure. If this interpretation is correct, one would expect that the substitution of the C–H eclipsed bond by a C–F bond, which enhances the hyperconjugative interaction, will stabilize the eclipsed rotamer

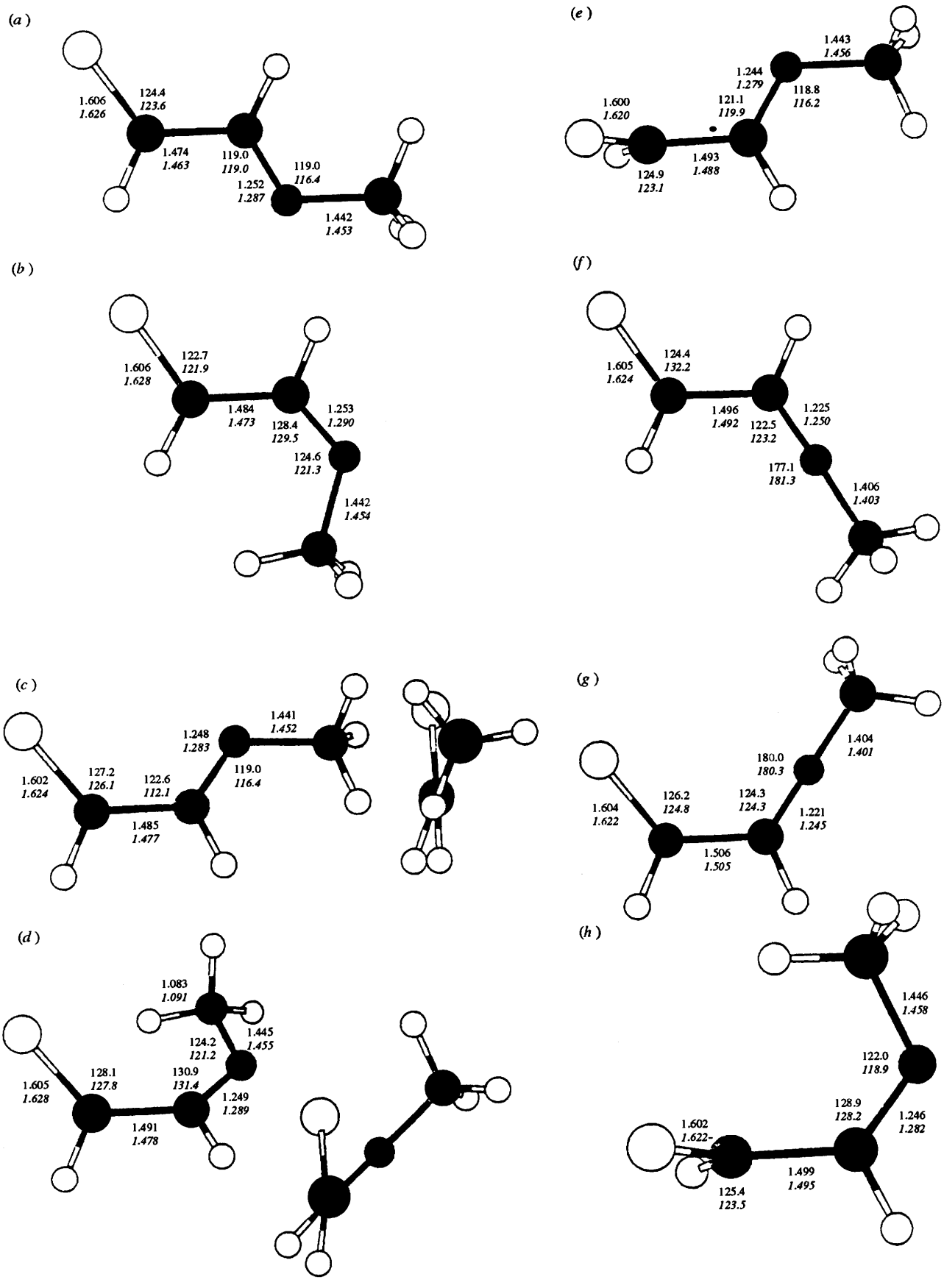

Fig. 1 HF/6-31G(d,p) and MP2/6-31G(d,p) (italic) optimized geometrical parameters of the equilibrium and transition structures for the **3a**(*trans*,s-*trans*) ⟶ **3a**(*cis*,s-*cis*) isomerization: bond lengths in Å, angles in degrees. (*a*) **3a**(*trans*,s-*trans*), (*b*) **3a**(*trans*,s-*cis*), (*c*) **3a**(*cis*,s-*trans*), (*d*) **3a**(*cis*,s-*cis*), (*e*) **TS1** (161i), (*f*) **TS1′** (467i), (*g*) **TS2** (432i), (*h*) **TS2′** (90i).

Table 1 Zero-point energies (ZPVE) (kcal mol^{-1}) and relative energies (kcal mol^{-1}) of the (C_3H_5NS) stationary points considered at different levels of theory

Point	ZPVE[a] energy	Relative energy					
		HF[b]	MP2[c]	MP2[c,d]	MP4SDTQ[c,d]	QISD(T)[c,d]	MP4 + ZPVE[e]
3a(*trans*,s-*trans*)	45.6	0.0	0.0	0.0	0.0	0.0	0.0
3a(*trans*,s-*cis*)	45.4	6.4	5.2	5.3	5.0	6.2	4.8
3a(*cis*,s-*trans*)	45.7	6.5	5.3	5.6	5.4	—	5.5
3a(*cis*,s-*cis*)	45.6	10.3	8.2	8.7	8.2	8.6	8.2
2a(*gauche*)	44.1	8.3	9.9	8.8	9.4	—	7.9
2a(s-*trans*)	44.2	4.4	7.1	6.4	6.8	—	5.4
2a(s-*cis*)	44.3	2.7	4.9	4.0	4.6	—	3.3
8a(s-*trans*)	46.5	18.7	13.3	12.3	14.4	—	15.3
8a(s-*cis*)	46.8	22.5	17.1	15.7	17.7	—	18.9
1a	47.3	−3.2	−4.7	−6.4	−3.8	—	−2.1
7a	47.1	−15.5	−16.7	−16.2	−14.2	—	−12.7
TS1	45.1	8.5	8.1	7.5	7.1	—	6.6
TS1'	44.4	31.0	32.0	32.3	32.5	32.6	31.3
TS2	44.3	34.1	34.3	34.8	34.8	35.0	33.5
TS2'	45.2	10.9	9.8	9.6	9.2	—	8.8
TS3	42.8	54.7	31.7	30.8	35.0	37.1	32.2
TS4	43.8	8.9	11.5	10.3	10.8	—	9.0
TS5	43.9	7.4	11.4	10.7	11.0	—	9.3
TS6	43.0	29.4	19.5	19.0	21.8	—	19.2
TS7	46.2	32.0	37.6	34.0	35.3	—	35.9
TS8	46.4	26.5	21.8	19.9	21.6	—	22.4
TS9	43.3	98.3	71.1	71.7	72.4	—	70.1

[a] From HF/6-31(d,p) harmonic vibrational wavenumbers and scaled by 0.89. [b] Based on HF/6-31G(d,p) geometries. [c] Based on MP2(fc)/6-31G(d,p) geometries. [d] With the 6-31 + G(d,p) basis set; core orbitals are frozen. [e] Including MP4 relative energies and zero-point vibrational energies.

Table 2 Energy contributions of $n_N \rightarrow \sigma^*_{CX}$ delocalization and energy differences between eclipsed and staggered conformations of $S(CH)_2NCH_2X$, X = H and F[a]

	X = H		X = F	
	Eclipsed	Staggered	Eclipsed	Staggered
$n_N \rightarrow \sigma^*_{CH}$[b]	−0.4	−2.2	−0.4	−1.8
$n_N \rightarrow \sigma^*_{CX}$	−7.7	−2.6	−13.3	−8.7
Σ[c]	−8.5	−7.1	−14.0	−12.7
ΔE_{del}[e]	0.0	4.8	0.0	8.5
ΔE_{Lew}[d]	0.0	−2.8	0.0	−3.5
ΔE	0.0	2.0	0.0	5.0

[a] Energies are in kcal mol^{-1}. [b] There are two identical orbital interactions of this type, the CH bonds lying above and below the C=N–C(CH_2X) plane. [c] Total of the energies for the individual lone pair to vicinal CH(X) antibond delocalizations. [d] Difference in the energies of the Lewis structure obtained by setting all orbitals' interactions to zero. [e] Difference in delocalization energies ($\Delta E_{del} = \Delta E_{tot} - \Delta E_{Lew}$).

and increase the rotational barrier. Calculations have been performed for the *trans*,s-*trans* fluorine derivative S=CH–CH=N–CH_2F. There is a total of four different structures corresponding to stationary points on the HF/6-31G(d,p) potential energy surface. As expected, the C–F and C=N bonds are eclipsed in the most stable conformation. In the other stable structure a C–H bond eclipses the C=N one. The two staggered rotamers (C–F or C–H and C=N *anti*) are identified as first-order saddle points. The energy difference between the eclipsed (CF) and staggered (CF) conformations is equal to 5.0 kcal mol^{-1}. In order to definitively check our hypothesis, we have carried out a Fock matrix analysis with the NBO program [14] for the *trans*,s-*trans* S=CH–CH=N–CH_2X (X = H, F) compounds. Orbital interactions of interest (nitrogen lone pair and antibond σ^*_{CX} orbitals of CH_2X group) were calculated by setting the corresponding off-diagonal Fock matrix elements to zero. The results are summarized in Table 2. As predicted, the NBO analysis indicates the importance of $n_N \rightarrow \sigma^*_{CX}$ hyperconjugation when C–X and C=N are eclipsed and this contribution increases significantly for X = F. However, a close examination of Table 1 shows that the variation of the sum Σ of these interactions is almost constant whatever X and does not parallel ΔE_{del}. Hence, the energy difference between eclipsed and staggered structures cannot be rationalized quantitatively by $n_N \rightarrow \sigma^*_{CX}$ orbital interactions alone.

The most stable **3a** isomer is the *trans*,s-*trans* one (see Table 1) and the order of stability is the same whatever the level of calculations. There are two possible pathways from **3a**(*trans*,s-*trans*) to **3a**(*cis*,s-*cis*) (Fig. 2). The first involves a rotation about the C–C bond giving the *trans*,s-*cis* rotamer *via* the transition state **TS1** (Fig. 1) followed by inversion at the nitrogen atom forming the *cis*,s-*cis* compound *via* **TS2**. In the second pathway, inversion at nitrogen occurs first *via* **TS1'** and is followed by rotation about the C–C bond *via* **TS2'**. **TS1** and **TS2'** are reached for a ∠SCCN dihedral angle of about 90°; only **TS2** has the C_s symmetry; the CNC(H_3) bond angle is close to 180° in both **TS1'** and **TS2**. Table 3 reports the energy barriers of these steps. It appears that (*i*) barrier levels are reasonably well predicted at the HF level, the correlation corrections make little differences; this result can be related to the fact that, in the corresponding transition structures, no bond is partially broken or formed. (*ii*) The barrier heights for the inversion at nitrogen are, as expected, substantial (*ca.* 30 kcal mol^{-1}); similar results were obtained by Pople *et al.* in their study of the potential energy surface of H_2C=NH.[16] (*iii*) At the best level of calculation [ZPE/QCISD(T)/6-31 + G(d,p)] the inversion at the nitrogen of the *trans*,s-*trans* isomer constitutes the most energy-demanding step.

From 3a(*cis*,s-*cis*) to the enethiol 2a

Fig. 3 displays selected HF and MP2 parameters of stationary points relevant to this process. **TS3** is the transition structure for the [1,5]-sigmatropic hydrogen shift connecting **3a** and **2a**. IRC calculations at the 6-31G(d,p) level revealed that this transition state connects exactly the **3a**(*cis*,s-*cis*) and **2a**(*gauche*) isomers.

Table 3 Energy barriers $\Delta E^{\ddagger}$ (kcal mol^{-1}) and activation energy (kcal mol^{-1}) of the steps involved in the α-iminothioaldehyde rearrangement

	$\Delta E^{\ddagger}$					
	HF[a]	MP2[b]	MP2[b,c]	MP4SDTQ[b,c]	QCISD(T)[b,c]	Activation energy[d] MP4(QCISD)
TS1	8.5	8.1	7.5	7.1	—	6.6
TS1'	31.0	32.0	32.3	32.5	32.6	31.3 (31.4)
TS2	27.7	29.1	29.5	29.7	28.8	28.7 (27.8)
TS2'	4.4	4.6	4.4	4.1	—	3.3
TS3	44.4	23.5	22.0	26.8	28.5	24.0 (25.7)
TS4	1.4	1.6	1.6	1.4	—	1.5
TS5	3.0	4.4	4.3	4.2	—	3.9
TS6	26.6	14.6	15.0	17.1	—	15.9
TS7	13.3	24.4	21.7	20.9	—	20.6
TS8	4.0	4.7	4.2	4.0	—	3.5
TS9	101.5	71.1	71.7	72.4	—	72.2

[a] Based on HF/6-31G(d,p) geometries. [b] Based on MP2/6-31G(d,p) geometries. [c] With the 6-31 + G(d,p) basis set; core orbitals are frozen. [d] Including zero-point vibrational energies.

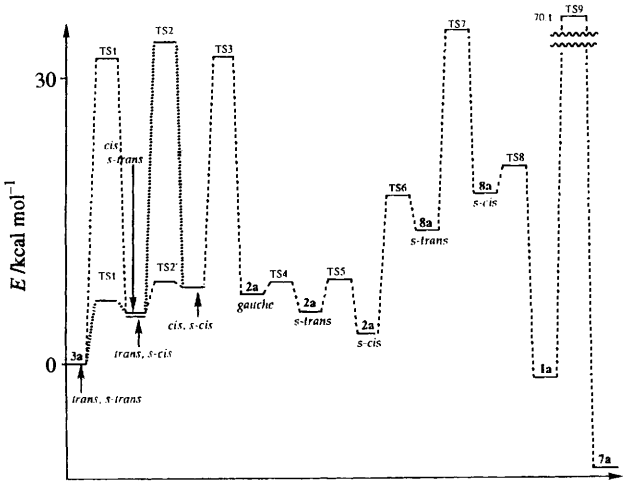

Fig. 2 Theoretical estimates of the relative energies at the MP4/6-31 + G(d,p) level for the whole process from **3a**(*trans*,s-*trans*) to **8a**

The main difference between HF and MP2 geometries concern the lengths of forming and breaking bonds which are 0.05 Å shorter at the MP2 level. Therefore, the transition state is predicted to be more tightened at this level. Pauling bond orders[17] n_p provide a useful measure of the extent of bond making (bm) and bond breaking (bb) in the transition structures, $\mathrm{Ln}(n_p/n_0) = (d_0 - d)/0.3$, where d and d_0 are the C(H_2) H bond lengths respectively in **TS3** and **3a**(*cis*,s-*cis*) and S–H bond lengths in **TS3** and product for bond making; n_0 is equal to 1 for single bonds. n_p(bb) Values of 0.346 (HF) and 0.426 (MP2) are calculated. The n_p(bm) values are lower, slightly at the HF level (0.327), more at the MP2 level (0.332). Bond index values are not decisive to determine the 'lateness' of **TS3**.

Further information concerning **TS3** can be obtained using the natural bond analysis (NBO) and natural localized molecular orbital analysis (NLMO) methods.[18] The principal resonance structure possesses a covalent S–H bond and the NLMO bond orders,[19] which give a covalent contribution to bonding, are equal to 0.512 for the bond between the sulfur atom and the migrating H and only 0.291 for the bond between this H and the carbon atom. It can be concluded that **TS3** resembles the product more than the reactant. This conclusion is further supported by the IRC calculations. From the values of the net reaction coordinate (s = 0 corresponds to the transition structure) for the *cis*,s-*cis*-α-iminothioaldehyde (s = 9.05) and the *gauche*-enethiol (s = −7.55) it becomes apparent that **TS3** is structurally closer to the enethiol than to the thioaldehyde. At the HF/6-31G(d,p) level, **2a**(*gauche*) lies 2.0 kcal mol^{-1} below **3a**(*cis*,s-*cis*) in energy. When correlation is introduced, a reverse order is obtained. However, when ZPVE correction is taken into account, this rearrangement is found to be nearly athermic (−0.3 kcal mol^{-1} at the MP4SDTQ + ZPVE level).

A barrier of 44.4 kcal mol^{-1} was calculated for this step at the HF/6-13G(d,p) level. As expected, when correlated methods which provide a more realistic description of the bond-breaking and -making processes were used, the barrier was significantly lowered (see Table 3). It is noteworthy that, at each level of theory, the barrier is substantially lower than that calculated for the [1,5]-hydrogen shift in (*Z*)-penta-1,3-diene (which varies in the range 36.5 (MP2)–58.1 (HF) kcal mol^{-1}).[20] At the higher level of theory, the activation energy was calculated to be 25.7 kcal mol^{-1}, lower than that of the limiting **3a**(*trans*,s-*trans*) ⟶ **3a**(*cis*,s-*trans*) step (31.4 kcal mol^{-1}). This result is in agreement with an expected rapid [1,5]-sigmatropy.

As mentioned previously, IRC calculations indicate that the product resulting from the [1,5]-sigmatropy is the *gauche*-enethiol. We have located two other stable conformers of **2a** each having a C_s symmetry (Fig. 3). The s-*trans* rotamer is predicted to be more stable than the gauche one by 2.5 kcal mol^{-1} (MP4 + ZPVE level) and the absolute minima of **2a** is the s-*cis* rotamer which lies 2.1 kcal mol^{-1} below the s-*trans* rotamer. The **2a**(*gauche*) ⟶ **2a**(s-*trans*) rotational barrier (**TS4**) is low (*ca.* 1.5 kcal mol^{-1} at both levels of calculation). **TS4** is reached by rotation around both C–S and C–N bonds. Thus in **2a**(*gauche*), the ∠HSCC and ∠CNCC dihedral angles are 141.4° and 53.4°, respectively (MP2). These values become 165.9° and 99.0° (MP2) in **TS4**. **2a**(s-*cis*) is obtained *via* **TS5**. This step proceeds with an activation barrier of about 4.0 kcal mol^{-1}. Consequently, the whole transformation **2a**(*gauche*) ⟶ **2a**(s-*cis*) is a facile step.

It is of interest to examine the origin of the largest stability of the s-*cis* isomer. The presence of an intramolecular N ··· H–S hydrogen bond seems to be a natural explanation and, for the s-*cis* isomer, a stronger nitrogen lone pair n_N–σ^*_{SH} interaction is expected.[18] Table 4 reports the main energy terms resulting from a NBO deletion procedure applied to the **2a** stable isomers. Surprisingly, the $n_N \rightarrow \sigma^*_{SH}$ is weak and its variation is not sufficient to explain the relative stabilities of **2a** isomers. Our results show that the whole delocalization energy E_{del} is the factor determining the stability of these rotamers.

From the enethiol 2a to the zwitterion 8a

The transition structure **TS6** (Fig. 4) describes the migration of the H atom from S (2–H bond) to N (N^+–H bond). At the two levels of geometry optimization, breaking and forming bond lengths are very close, as is the ∠SHN bond angle. In **TS6** the breaking S–H bond is 0.325 Å (HF) or 0.310 Å (MP2) longer

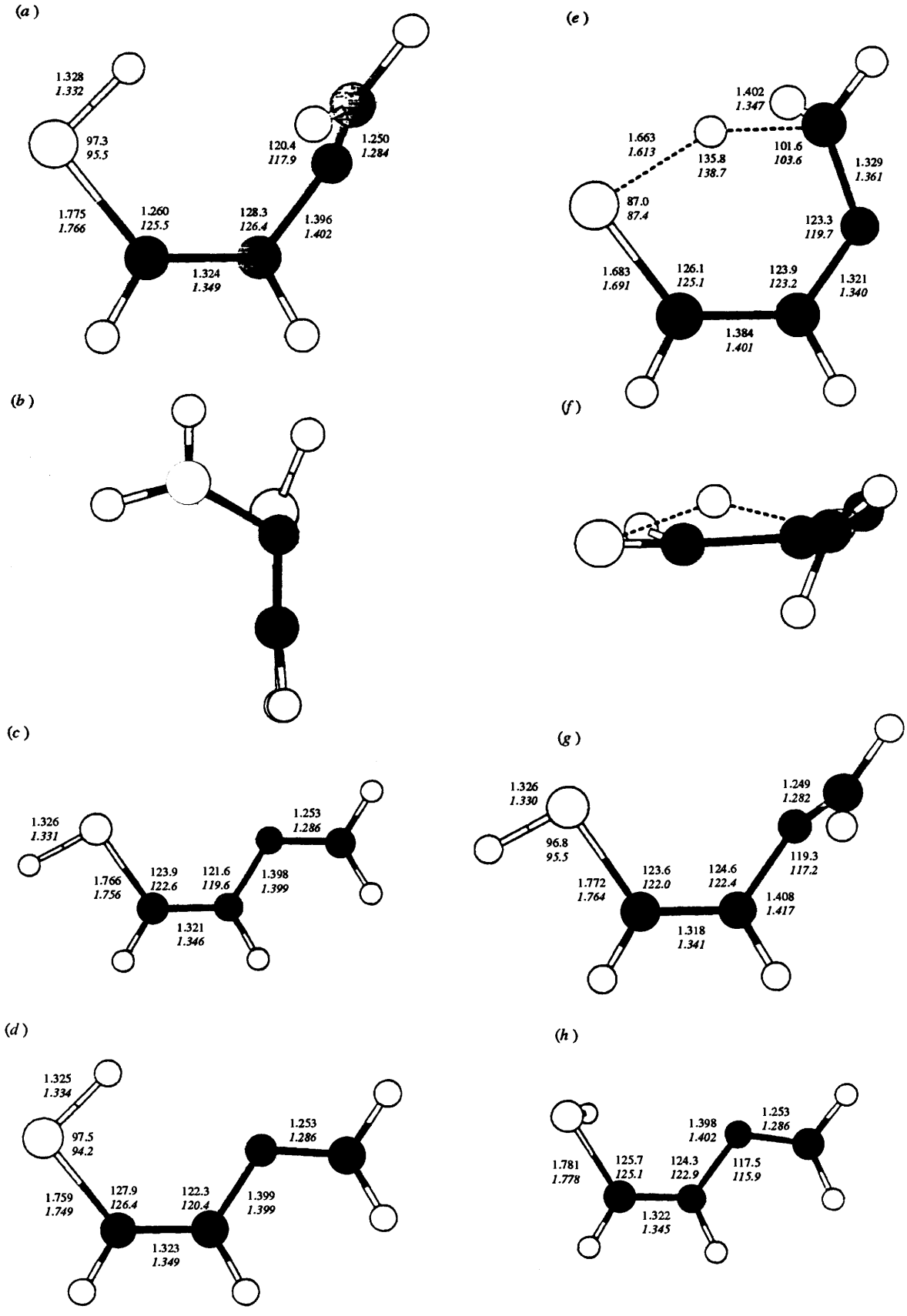

Fig. 3 HF/6-31G(d,p) and MP2/6-31G(d,p) (italic) geometrical parameters for the **3a**(*cis*,s-*cis*) ⟶ **2a** transformation. (*a*) **2a**(*gauche*), (*b*) **2a**(*gauche*), (*c*) **2a**(s-*trans*), (*d*) **2a**(s-*cis*), (*e*) **TS3** (2265i), (*f*) **TS3**, (*g*) **TS4** (114i), (*h*) **TS5** (226i).

than the corresponding bond in **2a**(s-*cis*). The forming N–H bond is 0.274 Å (HF) or 0.262 Å (MP2) longer than that of the zwitterion **8a**. The main feature of this transition state is its planarity which requires that the orbital interactions are qualitatively different from those encountered in pericyclic reactions. Despite a large lengthening of the S–H bond in this

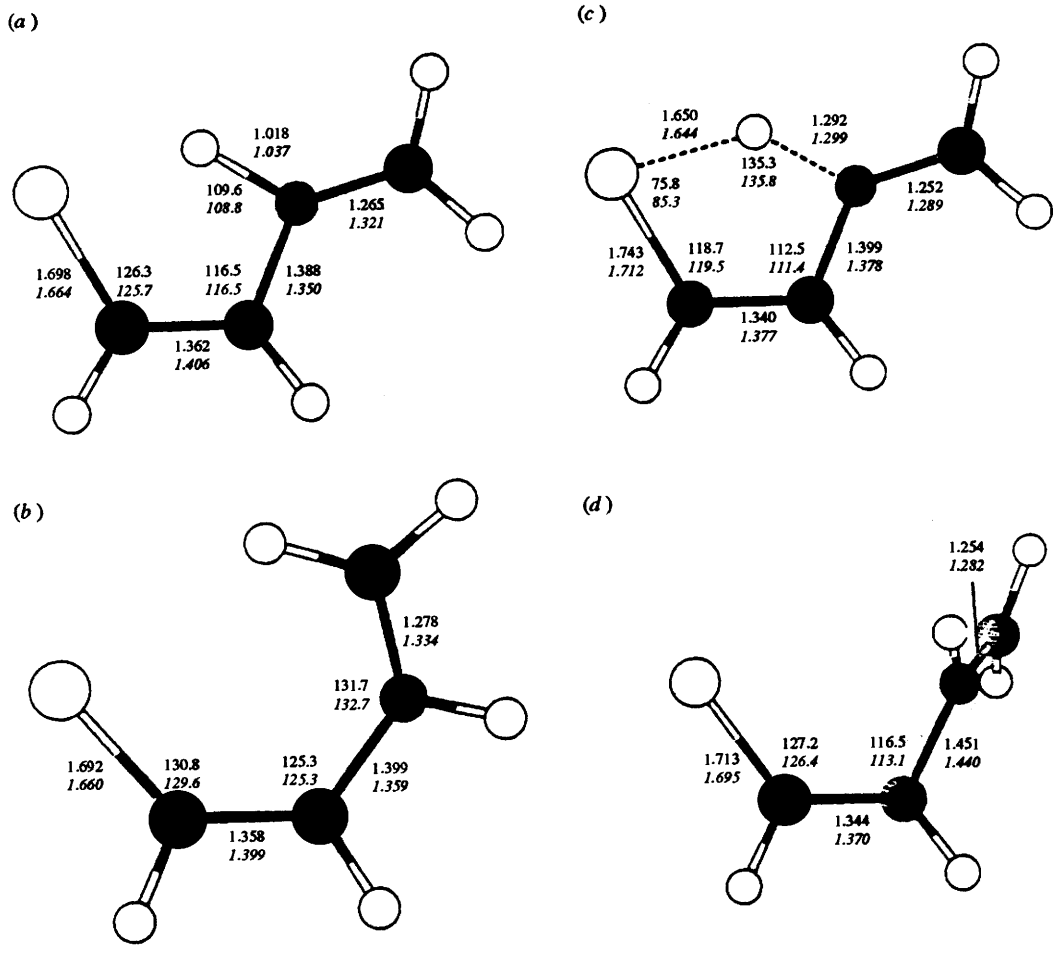

Fig. 4 HF/6-31G(d,p) and MP2/6-31(d,p) (italic) geometrical parameters for the **2a** ⟶ **8a** rearrangement. (*a*) **8a**(s-*trans*), (*b*) **8a**(s-*cis*), (*c*) **TS6** (1747i), (*d*) **TS7** (191i).

Table 4 Contributions (kcal mol^{-1}) of $n_N \rightarrow \sigma^*$ orbital interaction, delocalization as a total (ΔE_{del}) and Lewis energies (ΔE_{Lew}) to the energy differences (ΔE_{tot}) between the three **2a** isomers

	2a(*gauche*)	**2a**(s-*trans*)	**2a**(s-*cis*)
$n_N \rightarrow \sigma^*_{SH}$	0.0	−0.8	−1.3
E_{del}	−226.5	−227.8	−223.1
ΔE_{del}	5.6	4.3	0.0
ΔE_{Lew}	−0.5	−2.4	0.0
ΔE_{tot}	5.1	1.9	0.0

transition structure, NBO/NLMO analyses seem to indicate that TS6 is a rather early transition state: a S–H bond is present in the 'best' resonance structure and NLMO bond orders for S–H and N–H bonds are respectively 0.387 and 0.184. However, the IRC which is depicted for this process in Fig. 5, gives values of the net reaction coordinate equal to −5.67 for the reactant **2a** and to 3.08 for the product **8a**.

The IRC prediction of a transition state structurally close to **8a** than to **2a** can be related to the endothermicity of this process (+12.0 kcal mol^{-1} at the MP4 + ZPVE level) in accordance with the Hammond postulate. Thus, it appears that the difference between the geometric and electronic descriptions of bonds breaking and forming is stronger here.

The usual trends are observed in calculated energy barrier: MP2 underestimates it and MP4 begins to converge on a reasonable energy barrier (Table 3). The MP4(STDQ) + ZPVE energy of **TS6** is 15.9 kcal mol^{-1} above **2a**(s-*cis*), a value lower than the activation energy calculated for the [1,5]-sigmatropic shift.

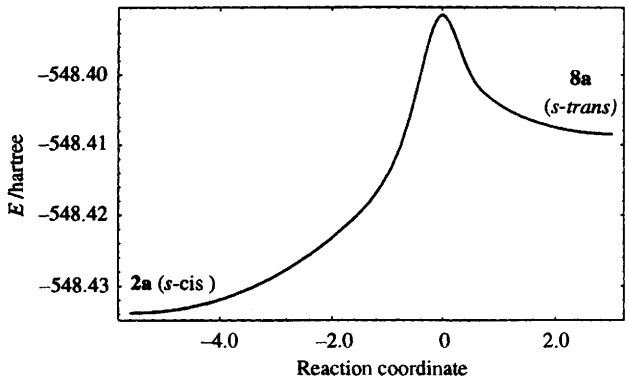

Fig. 5 Potential energy profile for the **2a** ⟶ **8a** rearrangement

Let us now comment on the structures of the intermediate **8a**. As mentioned previously, IRC revealed that **TS6** gives exactly the s-*trans* isomer. **TS7** is the transition structure which connects **8a**(s-*trans*) and **8a**(s-*cis*) (see Fig. 4). The salient result emerging from the data listed in Fig. 4 is that geometrical parameters depend strongly on the level of calculation. The most conspicuous changes are the shortening of the C–N and C–S bonds and the lengthening of the C=C and N=C bonds when electron correlation corrections were included by MP2/6-31G(d,p) geometry optimizations. These modifications reveal changes in the π-character of these bonds and suggest that the contribution of the polar canonical form **B** (Scheme 4) as a resonance structure of **8a** increases with correlation.

This analysis is supported by the NBO search of the Lewis

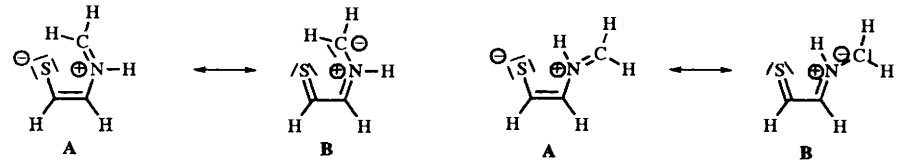

	A	B	A	B
HF:	0.7736	1.7388	0.7416	1.7128
MP2:	0.9256	1.5818	0.9036	1.5577

Scheme 4 Overall non-Lewis occupancies of the resonance structures **A** and **B** in **8a**(s-*cis*) and **8a**(s-*trans*)

structures. In Scheme 4 are reported for each structure the non-Lewis occupancies (the lower the non-Lewis density the better the corresponding structure is). When comparing these values, it can be concluded that, at the MP2 level, the participation of the resonance structure **B** to the description of **8a** is more important. As a result, the correlated rotational barrier around the C–N bond which lies in the range 20.9–24.4 kcal mol^{-1} is larger than that calculated at the HF level (13.3 kcal mol^{-1}).

Whatever the level of calculation, the s-*trans* intermediate is found to be more stable than its s-*cis* rotamer (energy difference = 3.3–3.8 kcal mol^{-1}). The NBO deletion procedure indicates that the former isomer is favoured by non-hyperconjugative effects, *e.g.* steric and electrostatic [ΔE_T = 3.5 kcal mol^{-1}, ΔE_{del} = −1.1 kcal mol^{-1}, ΔE_{Lew} = 4.6 kcal mol^{-1} at the HF/6-31 + G(3,p) level with MP2 geometries].

From the zwitterion 8a to the cycles 1a and 7a

The geometries of the main points of these paths are presented in Fig. 6. The cyclization of **8a**(s-*cis*) into **1a** occurs *via* the transition state **TS8**. This ring closure is exothermic by 21.0 kcal mol^{-1}. It is a facile step with an energy barrier of only 4.0 kcal mol^{-1}. This value varies little with the level of calculation. **TS8** is an early transition state with the S···C(5) length very extended [2.818 Å (HF) and 2.760 Å (MP2)] and the N–C(5) bond displaying essentially double bond character (1.337 Å *vs.* 1.334 Å in the reactant and 1.454 Å in the product at the MP2 level). IRC calculations (s = 5.16 for the reactant **8a**, s = 6.45 for the cyclic product **1a**) as well as NBO/NLMO analysis [S···C(5) bond order equal to 0.111 in **TS8** and to 0.887 in **1a**] support the geometrical predictions.

The ring closure leads to a conformer of **1a** having an axial N–H bond (verified by the IRC calculation). The equatorial form is less stable than the axial one by 0.5 kcal mol^{-1} [MP4STDQ/6-31 + G(d,p) + ZPE//MP2/6-13G(d,p)].

Finally, we will consider the last step of this rearrangement, the [1,3]-sigmatropic H(10) shift, which experimentally occurs in $CDCl_3$ solution. The symmetry forbidden suprafacial migration is expected to be an unfavourable pathway. The first order transition structures **TS9** (Fig. 6) was located at the HF/6-31G(d,p) level. However, the standard procedure at the MP2/6-31G(d,p) level failed to converge on a transition structure. Due to the size of the system and prohibitive memory size requirements, it was unpractical to obtain MP2/6-31(G(d,p) second derivatives and, instead, a directed grid search was used. The N–H(10) and C(2)–H(10) bonds were fixed and the other geometrical parameters were optimized. The forces of the fixed bonds and the total energy were used to direct the search. A conservative estimate would be that the bond lengths are optimized within the range 0.01–0.02 Å. There is a large discrepancy between some HF and MP2 bond lengths, but the two methods agree on a short C(1)–H(10) distance in the transition structure [1.190 Å (HF), 1.296 Å (MP2)]. Consequently, it is not obvious that H(10) in **TS9** transfers to N during the reaction. For this reason, we made use of the HF/6-31G(d,p) **TS9** geometry to calculate the IRC. The distances between

Table 5 Distances (in Å) between the migrating H(10) and N, C(1) and C(2) for several points selected along the IRC for **1a** ⟶ **7a** rearrangement

Net reaction coordinate s	Distance[a]		
	H(10)–N	H(10)–C(1)	H(10)–C(2)
−2.94 (**1a**)	1.002	2.009	2.937
−1.60	1.057	1.491	2.140
−0.60	1.304	1.261	1.834
−0.20	1.464	1.203	1.697
0.00 (**TS9**)	1.549	1.190	1.630
0.20	1.635	1.189	1.566
0.40	1.720	1.200	1.503
0.80	1.885	1.253	1.379
1.20	2.039	1.343	1.263
2.80	2.610	1.861	1.091
4.00	2.948	2.081	1.085
4.49 (**7a**)	2.980	2.071	1.082

[a] Atoms' numbering, see Fig. 6.

H(10) and the N, C(1) and C(2) centres for various values of the net reaction coordinate are given in Table 5. It appears clearly that **1a** and **7a** are connected *via* **TS9**. It is also of interest to notice that in the range from s = −0.2 to s = +0.4, the *C*(1)–H(10) distance remains almost constant while the other two distances vary noticeably in the meantime. The principal resonance structure found by the NBO search is shown in Scheme 5. It is consistent with the results given by the natural population analysis [NPA charges at N(3) and H(10) are respectively −0.749 and +0.532]. Calculated NLMO/NPA bond orders are 0.103 [H(10)–N], 0.462 [H(10)–C(1)] and 0.251 [H(10)–C(2)]. Again in this case variations of bond orders do not parallel closely geometrical trends [in view of elongation of bonds in **TS9**, a value of 0.251 for the H(10)–C(2) bond is unexpected].

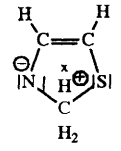

Scheme 5

The final product **7a** is more stable than **1a** by 10.6 kcal mol^{-1}. Despite the exothermicity of this step, its activation energy was calculated to be large (72.2 kcal mol^{-1}). Thus, a thermal **1a** ⟶ **7a** rearrangement is very unlikely. This enamine ⟶ imine rearrangement is most probably not a unimolecular process.[5]

Conclusions

Fig. 2 summarizes the mechanism and energetics for the overall process. Apart from the last **1a** ⟶ **7a** step, the highest

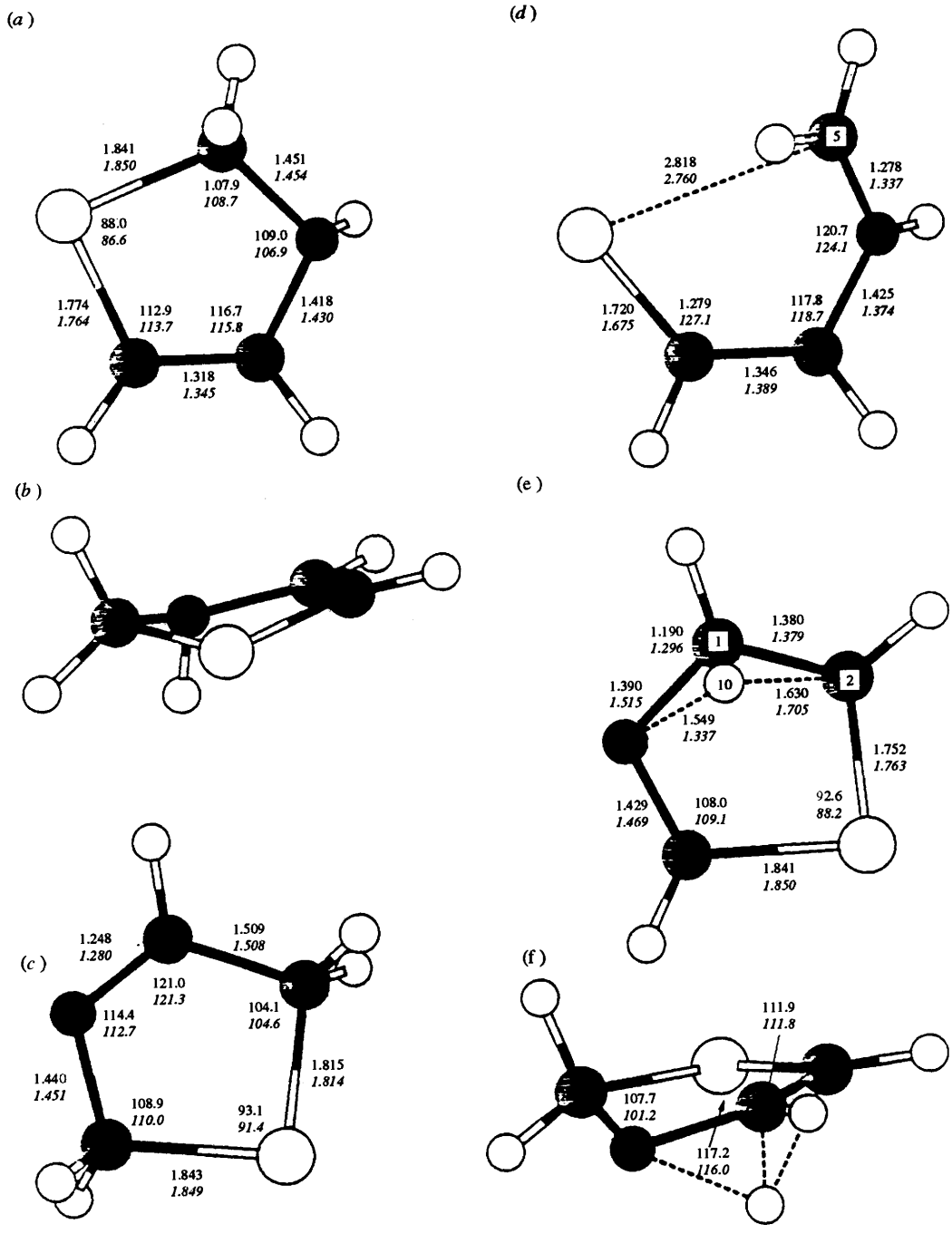

Fig. 6 HF/6-31G(d,p) and MP2/6-31G(d,p) (italic) geometrical parameters for the cyclization step. (*a*) **1a**, (*b*) **1a**, (*c*) **7a**, (*d*) **TS8** (195i), (*e*) **TS9** (1935i), (*f*) **TS9**.

calculated barriers correspond to the **3a**-*trans* ⟶ *cis* isomerization and to the (1,5)-sigmatropic shift leading to the enethiol **2a**(*gauche*). At our best level of theory, *i.e.* QCISD(T)/6-31 + G(d,p)//MP2/6-31G(d,p) + ZPVE corrections, the activation energy of this second step was calculated to be lower (25.7 kcal mol^{-1}) than that of the first one (27.8 kcal mol^{-1}, see Table 3). Thus, the *trans* ⟶ *cis* isomerization constitutes the most energy requiring step. Figs. 1, 3, 4 and 6 list the unscaled imaginary frequencies of all the transition structures. For **TS2**, the absolute value of the reaction coordinate frequency (431i) is much lower than that calculated for **TS3** (2265i). To the extent that the Wigner and Bell methods for approximating tunnelling effect[21] are a reasonable picture of physical reality, a larger tunnel correction is expected for the sigmatropic [1,5]-hydrogen migration.

Experimental

12-Formyl-9,10-dimethyl-9,10-dihydro-11-thia-9,10-ethano-anthracene

Compound **5**[9] (5 g; 18 mmol) was dissolved in dry toluene (280 cm^3) at 0 °C. A 1.5 mol dm^{-3} solution of DIBAL-H in toluene (54 mmol) was then added dropwise. The reaction mixture was stirred from 0 °C to room temperature for 12 h. After cooling back to 0 °C, the hydrolysis was performed with hydrochloric acid (1 mol dm^{-3}). The organic layer was separated and washed twice with water. Toluene was evaporated under reduced pressure and the resulting oil was submitted to column chromatography (eluent pentane–chloroform, 40:60). Yield 92%; mp: 120–130 °C (decomp.); $\nu(CDCl_3)/cm^{-1}$ 1700 (CHO); $\delta_H(CDCl_3$; 300 MHz) 2.16 and 2.34 (2 s, 6 H, Me), 3.50 (d, 1 H,

CH), 7.2–7.4 (m, 8 H, Ar) and 8.42 (d, 1 H, CHO); δ_C($CDCl_3$; 75 MHz) 17.26 and 18.29 (2 Me), 44.61 and 46.86 (C), 63.44 (CH), 118.91, 119.28, 121.90, 122.82, 126.26, 126.85, 127.11, 140.00, 142.63, 144.73 and 145.26 (Ar) and 195.98 (CHO); *m/z* 280 ($M^{\cdot+}$, 6%), 251 ($M^{\cdot+}$ − CHO, 1), 206 (dimethylanthracene$^{\cdot+}$, 100), 191 (methylanthracene$^+$, 60), 178 (anthracene$^{\cdot+}$, 12), 74 ($M^{\cdot+}$ − DMA, 3) and 45 (10) (HRMS Calcd. $C_{18}H_{16}OS$; 280.0922 Found: 280.0922).

12-(*N*-Methyliminomethyl)-9,10-dimethyl-9,10-dihydro-11-thia-9,10-ethanoanthracene (4a)

Gaseous methylamine was bubbled for 2 h at 0 °C through a solution of 12-formyl-9,10-dimethyl-9,10-dihydro-11-thia-9,10-ethanoanthracene (1 mmol) in dichloromethane (5 cm^3) containing molecular sieves (4 Å). The solvent was evaporated under reduced pressure. Compound **4a** was obtained in quantitative yield. No aldehyde was detected in the NMR and IR spectra. Mp 125–130 °C (decomp.); ν($CDCl_3$)/cm^{-1} 1656 (C=N); δ_H($CDCl_3$; 300 MHz) 2.07 and 2.28 (2 s, 6 H, Me), 3.14 (d, 3 H, Me, J = 1.5 Hz), 3.75 (d, 1 H, CH, J = 8.3 Hz), 6.67 (dq, 1 H, CH, J = 1.5 and 8.3 Hz) and 7.1–7.5 (m, 8 H, Ar); δ_C($CDCl_3$; 75 MHz) 17.54 and 18.25 (2 Me), 45.37 and 44.61 (2 C), 47.27 (MeN), 59.78 (CH), 118.86, 119.06, 122.13, 123.24, 126.04, 126.18, 126.64, 126.85, 141.12, 143.83, 145.42 and 145.70 (Ar) and 163.69 (C=N) (HRMS Calcd. $C_{19}H_{19}NS$; 293.1238. Found: 293.1230).

12-(*N*-Isopropyliminomethyl)-9,10,dihydro-11-thia-9,10-ethanoanthracene (4b)

A solution of isopropylamine (1 mmol) in dichloromethane (5 cm^3) containing molecular sieves was cooled to 0 °C. 12-Formyl-9,10-dimethyl-9,10-dihydro-11-thia-9,10-ethanoanthracene (1 mmol) dissolved in dichloromethane (5 cm^3) was added dropwise and the reaction was carried out for 8 h. After filtration and evaporation of the solvent, the desired imine was obtained in quantitative yield. No aldehyde was detected in its NMR and IR spectra. Mp 116–121 °C (decomp.); ν($CDCl_3$)/cm^{-1} 1650 (C=N); δ_H($CDCl_3$; 300 MHz) 1.02 and 1.16 (2 d, 6 H, 2 *Me*-isopropyl), 2.08 and 2.28 (2 s, 6 H, Me), 3.15 (m, 1 H, C*H*-isopropyl), 3.73 (d, 1 H, CH), 6.64 (d, 1 H, CH) and 7.1–7.4 (m, 8 H, Ar); δ_C($CDCl_3$, 75 MHz) 17.34 and 17.86 (2 Me), 23.61 and 24.33 (2 *Me*–isopropyl), 45.37 and 44.61 (2 C), 59.33 and 60.63 (2 CH), 118.68, 118.89, 122.97, 125.82, 126.00, 126.42, 126.65, 141.08, 143.73, 145.25 and 145.64 (Ar) and 159.76 (C=N) (HRMS Calcd. $C_{21}H_{23}NS$, 321.1551 Found: 321.1550).

FVT of compounds 4a and b

50 mg samples of imine **4a** or **b** were sublimed under 10^{-5} hPa through an empty quartz tube (l = 20 cm, i.d. = 1.6 cm) heated at 500 °C (the FVT apparatus has been described elsewhere [4,6,22]). DMA was separated by crystallization at the oven exit. The other products were condensed at −196 °C on a frozen mixture of $CDCl_3$ and $CFCl_3$ (3:1), transferred upon melting in a NMR tube fitted below the cold trap, and immediately analysed by NMR spectroscopy at −60 °C (Bruker 250 apparatus), then at room temperature. The NMR spectra of the obtained dihydrothiazoles are reported in Scheme 3. IR data were reported in the preliminary communication.[4]

References

1 R. Tanaka and I. Shinkai, in *Progress in Heterocyclic Chemistry*, ed. H. Suschitzky and E. F. V. Scriven, Pergamon, Oxford, 1993, vol. 5, pp. 159–172.
2 J. M. Sprague and A. H. Land, in *Heterocyclic Compounds*, ed. R. C. Elderfield, Wiley, New York, 1957, vol. 5, pp. 484–722.
3 H. Vorbrüggen, *Tetrahedron Lett.*, 1968, 1631; D. W. Young, D. J. Morecombe and P. K. Sen, *Eur. J. Biochem.*, 1977, **75**, 133; A. Kleemann, J. Martens, H. Bethge and P. Scherberich, EP Appl. 44,010/1982 (*Chem. Abstr.*, **96**, 199671).
4 Preliminary communication, R. Arnaud, N. Pelloux-Léon, J.-L. Ripoll and Y. Vallée, *Tetrahedron Lett.*, 1994, **35**, 8389.
5 J.-L. Ripoll, H. Lebrun and A. Thuillier, *Tetrahedron*, 1980, **36**, 2497.
6 G. Pfister-Guillouzo, F. Gracian, A. Senio, F. Bourdon, Y. Vallée and J.-L. Ripoll, *J. Am. Chem. Soc.*, 1993, **115**, 324; F. Bourdon, J.-L. Ripoll, Y. Vallée, S. Lacombe and G. Pfister-Guillouzo, *J. Org. Chem.*, 1990, **55**, 2596.
7 R. F. C. Brown, *Pyrolytic Methods in Organic Chemistry*, Academic Press, New York, 1980.
8 M.-C. Lasne and J.-L. Ripoll, *Synthesis*, 1985, 121.
9 N. Pelloux, Y. Vallée and V. Duchenet, *Phosphorus Sulfur Silicon*, 1994, **89**, 17; G. W. Kirby, *Phosphorus Sulfur Silicon*, 1993, **74**, 17.
10 H. Vorbrüggen, *Helv. Chim. Acta*, 1991, **74**, 297.
11 Gaussian92, Revision A. M. J. Frisch, G. W. Trucks, M. Head-Gordon, P. M. W. Gill, M. W. Wong, J. B. Foresman, B. G. Johnson, H. B. Schlegel, M. A. Robb, E. S. Reploge, R. Gomperts, J. L. Andres, K. Raghavachari, J. S. Binkley, C. Gonzalez, R. L. Martin, D. J. Fox, D. J. Defrees, J. Baker, J. J. P. Stewart and J. A. Pople, Gaussian Inc., Pittsburg, 1992.
12 W. J. Hehre, L. Radom, P. v. R. Schleyer and J. A. Pople, *Ab Initio Molecular Orbital Theory*, Wiley, New York, 1986.
13 (*a*) C. Gonzalez and H. B. Schlegel, *J. Chem. Phys.*, 1989, **90**, 2154; (*b*) 1990, **94**, 5523.
14 NBO Version 3.1, E. D. Glendening, A. E. Reed, J. E. Carpenter, F. Weinhold. For a description of this program, see: E. D. Glendening, A. E. Reed, J. E. Carpenter and F. Weinhold, NBO 3.0 Program Manual, QCPE Program No. 504.
15 (*a*) L. A. Curtiss, D. J. Poclatko, A. E. Reed and F. Weinhold, *J. Chem. Phys.*, 1985, **82**, 2679; (*b*) J. Tyrell, R. B. Weinstock and F. Weinhold, *Int. J. Quantum Chem.*, 1981, **19**, 781.
16 J. A. Pople, K. Raghavaclari, M. J. Frisch, J. S. Binkley and P. v. R. Schleyer, *J. Am. Chem. Soc.*, 1983, **105**, 6389.
17 L. Pauling, *J. Am. Chem. Soc.*, 1947, **69**, 542.
18 For a review of such methods, see A. E. Reed, L. A. Reed and F. Weinhold, *Chem. Rev.*, 1988, **88**, 899.
19 A. E. Reedland P. v. R. Schleyer, *J. Am. Chem. Soc.*, 1990, **112**, 1434.
20 For a review of transition structures in hydrocarbon pericyclic reactions, see: K. N. Houk, Y. Li and J. D. Evansek, *Angew. Chem., Int. Ed. Engl.*, 1992, **31**, 682.
21 R. P. Bell, *The Tunnel Effect in Chemistry*, Chapman and Hall, London, 1980.
22 Y. Vallée, *Rev. Heteroatom Chem.*, 1992, **6**, 1.

Paper 4/07514E
Received 8*th December* 1994
Accepted 19*th January* 1995